Estimating Seismic Hazard in the Basin and Range Province Using Horizontal GPS Data: Collaborative Research between the University of Nevada, Reno and the USGS

FINAL TECHNICAL REPORT
Award Number: 07HQGR0027

William C. Hammond, Corné Kreemer
University of Nevada, Reno
Reno, NV 89557-0178

whammond@unr.edu
Ph. 775-784-6436
Fax: 775-784-1709
http://geodesy.unr.edu

Submitted to the U.S. Geological Survey

March 31, 2008

1. Technical Abstract

We have used a compilation of horizontal GPS velocities to improve estimates of the pattern and rate of crustal strain in the western Basin and Range province (BRP). We model the strain with two complementary approaches. The first is a block methodology that represents the crust as an assembly of elastic spherical caps (lithosphere) that move over the Earth surface, and contact one another at faults that are locked at the surface but slip at depth. The second is a continuum tensor strain rate mapping technique that results in a relatively smooth representation of crustal strain.

The block strategy takes advantage of knowledge of the geometry of geologic structures that accommodate strain and produce earthquakes. We used selected active faults present in the USGS Quaternary Fault and Fold database (QFFD) and the published literature to define block geometries in a model of the western Basin and Range province. The resulting estimate provides kinematically self-consistent models of surface deformation that are consistent with knowledge of fault trace geometry, geodetically estimated rates of motion, transient earthquake cycle effects effecting the GPS deformation signal, and our best estimates for how faults behave at depth in the interseismic time frame. The fault slip rate estimates can be used to develop future versions of the National Seismic Hazard Maps (NSHM) that use slip rates on faults as a critical input.

Tensor strain rate mapping has the additional advantage that it can be used to make direct comparisons between geodetic and geologic measures of deformation. In this report we also compare the tensor strain rate maps obtained from the GPS measurements to similar maps obtain from geologic data, mostly in the form of fault slip rate estimates available in the published literature and the USGS QFFD. These show that deviations in the ratio between geodetic and geologic moment are most likely owing to 1) underestimate or lack of investigation of geologic slip rate on faults in the westernmost BRP/Sierra Nevada, 2) postseismic relaxation owing to historic earthquakes in central Nevada, 3) low values or lack of data for geologic moment that cause instability of the geodetic/geologic ratio calculation in the central BRP.

In past releases of the NSHM it was noted that the sum of geologically estimated slip rate estimates across active faults in the western BRP did not add up to the far-field geodetically determined motion of the Sierra Nevada microplate with respect to the central Basin and Range. This discrepancy was adjusted for by invoking simply shaped zones of shear that compensated for the "missing" geologic moment (*Frankel et al.,* 2002). Since that time geodetic studies have made significant advances in mapping the pattern and rate of deformation in the Basin and Range Province. These advances should be reflected in the shapes of any zones used to account for the discrepancy between geologically and geodetically inferred deformation rates. The continuum tensor strain rate models could be used as inputs into the NSHMs when knowledge of the specific faults that release the strain is not available.

2. Introduction

2.1 Horizontal GPS Velocity Data

To constrain the patterns and rates of crustal deformation we used a compilation of GPS velocities for the western United States that is a combination of data processed by ourselves and rates obtained from published studies of Basin and Range crustal deformation. This compilation was constructed using the methodology described in *Kreemer et al.,* (2008). A slightly earlier version is available via Internet links noted in *Kreemer and Hammond,* (2007). Input data for our own solution came from the continuously recording GPS sites of the BARGEN, PBO, CORS, BARD, and PANGA networks. We included data from our own semi-continuously and episodically measured sites of the MAGNET/NEARNET networks which can provide precise velocities in as little as two years (http://geodesy.unr.edu/networks).

For the continuous sites we used GPS data from January 1, 1997 to December 31, 2007, while data from MAGNET/NEARNET began in January 2004. These data were processed in our laboratory, obtaining for each site daily estimates of position coordinates with the GIPSY/OASIS II software package from the Jet Propulsion Laboratory in precise-point-positioning mode with carrier phase ambiguities resolved (bias-fixed) (*Blewitt,* 1989; *Zumberge et al.,* 1997), using the AMBIZAP algorithm (*Blewitt,* 2006). Sites with less than one year of data spanned by their time series were not considered since their velocity estimates are too uncertain to be useful for estimating strain patterns in the Walker Lane. Each daily non-fiducial solution is transformed into the Stable North America Reference Frame (SNARF v1.0 – *Blewitt et al., 2005*), and then site velocities are obtained from a regression of the residual time series. Thus rates shown in this report are with respect to stable North America.

To increase the number and geographic coverage of GPS rate data, we also included rates from other published studies of GPS measured deformation in the Basin and Range Province. Rates from studies were rotated and aligned with our own GPS velocity solution so that they refer to the same reference frame as the rates obtained for the continuous studies. See *Kreemer and Hammond*, (2007) for a list of studies included. We exclude data within 28 km of the Long Valley volcanic area in eastern CA, since much of the GPS site motion there is owing to transient volcanic processes rather than to secular crustal motion owing to tectonic deformation. We also exclude data from the Mojave Desert, southernmost Sierra Nevada/Great Valley microplate (SNGV), and southernmost Owens Valley because these rates are strongly effected by transient motions owing to the 1999 M7.1 Hector Mine, and 1992 M7.3 Landers earthquakes (see below for discussion).

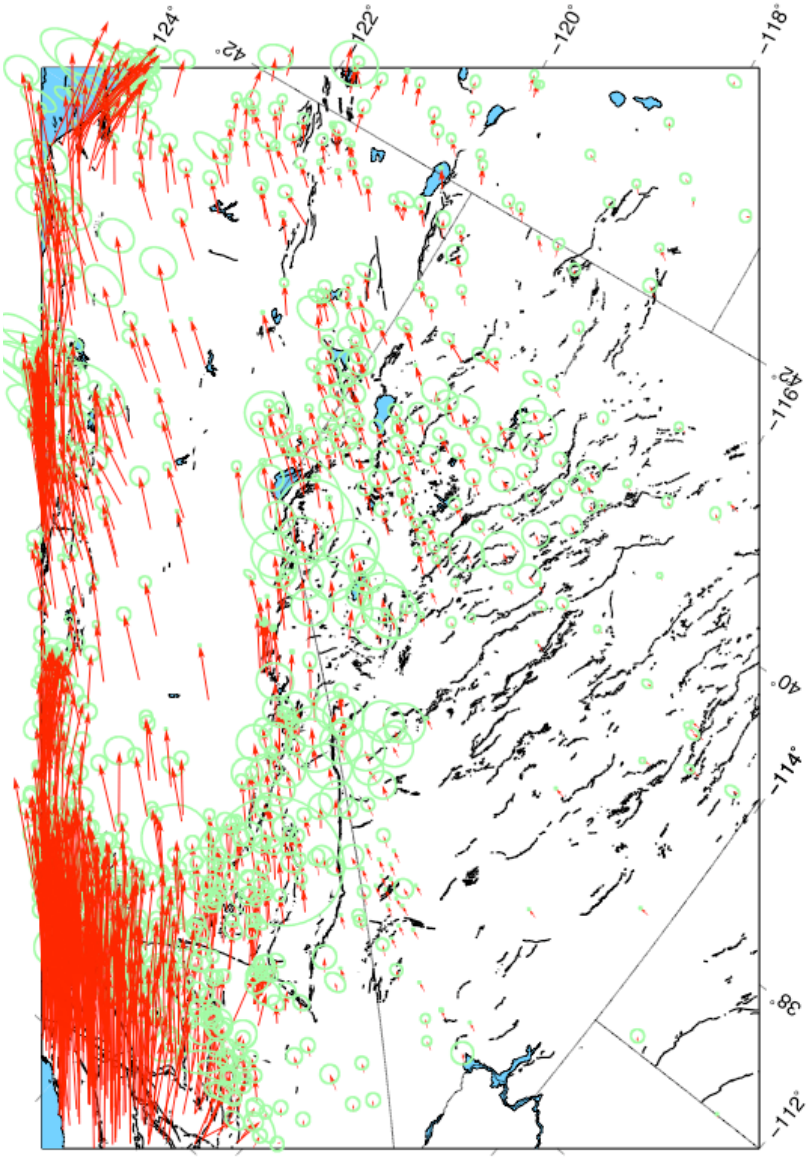

Figure 1. Horizontal GPS velocities for the western Unites States near our study area. 1-sigma uncertainties are indicated with the green ellipses. Figure is projected in Oblique Mercator around pole of relative motion between Pacific and North American plates. These velocities have not been adjusted for postseismic relaxation.

2.2. Correction for Postseismic Relaxation

In the 20th century a belt-like sequence of large (M>6.5) earthquakes occurred in central Nevada (*Bell et al.,* 2004). Stress changes from these Central Nevada Seismic Belt (CNSB) earthquakes appear to have induced a transient postseismic relaxation response in the lower crust and upper mantle that is characteristic of viscoelastic rheology of the lithosphere (*Hetland and Hager, 2003*; *Gourmelen and Amelung,* 2005). The magnitude of this response is on the order of a few mm/yr across the CNSB and has a strong effect on the interpretation of the modern GPS velocity field in terms of secular strain accumulation on faults. To separate strain accumulation (which is related to the long-term loading of faults) from the transient relaxation (which fades to zero over time) we have modeled the response of the earthquakes using the regional campaign and continuous GPS velocities and apply the correction to our GPS velocities (*Hammond et al.,* 2008). To illustrate the effect of this correction we show a close-up of the strain rate field estimated with and without the correction (Figures 2).

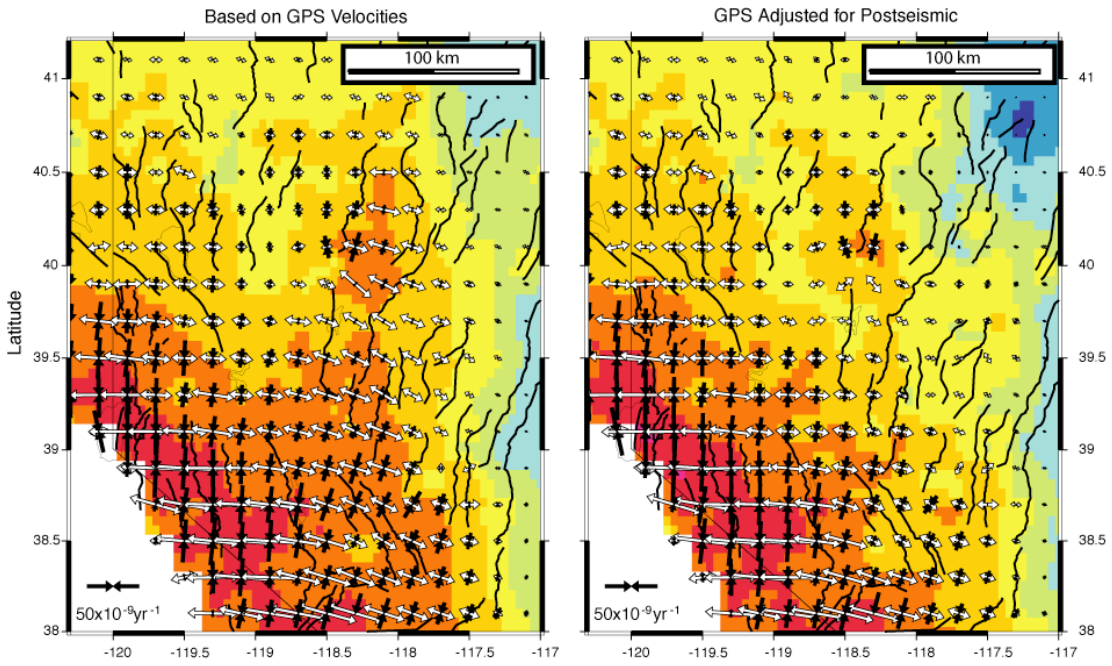

Figure 2. A strain map detail near the CNSB from (*Hammond et al.,* 2008). Postseismic relaxation following historic earthquakes at the Central Nevada Seismic Belt has a significant impact on the rate and style of inferred long-term deformation. A strain map based on the GPS velocities (left) and those velocities adjusted to account for the effects of relaxation (right) show very different strain rates in central Nevada near the epicenters of those earthquakes. Strain axes are black for contraction and white for extension.

We have not applied corrections to the velocity field for the M 7.1 Hector Mine, 1999, or the M7.3 1992 Landers earthquakes that occurred in the Mojave Desert. Although these events occurred outside the region we model, they are being followed by viscoelastic relaxation that is apparent in the GPS time series of sites near the earthquakes (*Deng et al.,* 1998; *Pollitz et al.,* 2001*; Pollitz,* 2003,), and sites that are > 100 km away from the epicenters (*Hammond et al.,* 2007; *Freed et al.,* 2007). Future versions of these models will have a correction for these

effects applied.

3. Results

3.1. Strain Maps

The strain maps shown in Figure 3 have been made using the continuum tensor strain rate mapping method (*Haines and Holt,* 1993; *Kreemer et al.,* 2000) with the correction for postseismic relaxation at the CNSB applied to the velocities. No part of the model has been assumed to be rigid. The highest strain rates are focused to the western part of the BRP and east of the SNGV, in agreement with earlier studies based on GPS geodesy. The width of the actively deforming zone is roughly 150 km, but varies in width from ~80 km (near latitude 37˚N km), widening substantially northward to >200 km (near latitude 40˚N). North of Walker Lane, in northeast CA, near the OR border with the strain patterns become discontinuous possibly owing to the much lower density of high quality continuous or semi-continuous GPS stations in that area.

The highest strain rate in the map occurs near latitude 38˚N, in the vicinity within 100 km of the Long Valley volcanic complex and the Mono Basin, north of Owens Valley. This concentration of strain occurs even though the model is obtained with sites in the immediate vicinity of Long Valley removed from the analysis. This may suggest that volcanic activity at Long Valley is somehow related to the organization and pattern of interaction between lithospheric blocks (however via cause or effect is unknown). The observation of high strains in this area is also present in the block models, presented below.

In the map, highest strain rates tend to occur where there are GPS sites, and lower strain rates occur where there are fewer sites. This is partially owing to sites being installed in locations where higher strain rates were thought to be occurring (observation selection bias), and partly owing to modeling constraints that favor zero strain in the absence of data. Zones in the model that have relatively low strain rates possibly because of lack of adequate GPS data include the area northwest of Lake Tahoe, which kinematic compatibility would suggest carries much of the slip on the eastern edge of the SNGV. This issue is addressed in the comparison between strain mapping and block modeling (discussed below). Also in southern Nevada a band of 4-8 nanostrains is present that may be related to southern Nevada seismicity and relative motion between the Colorado Plateau and Central BRP (*Kreemer et al.,* 2008b).

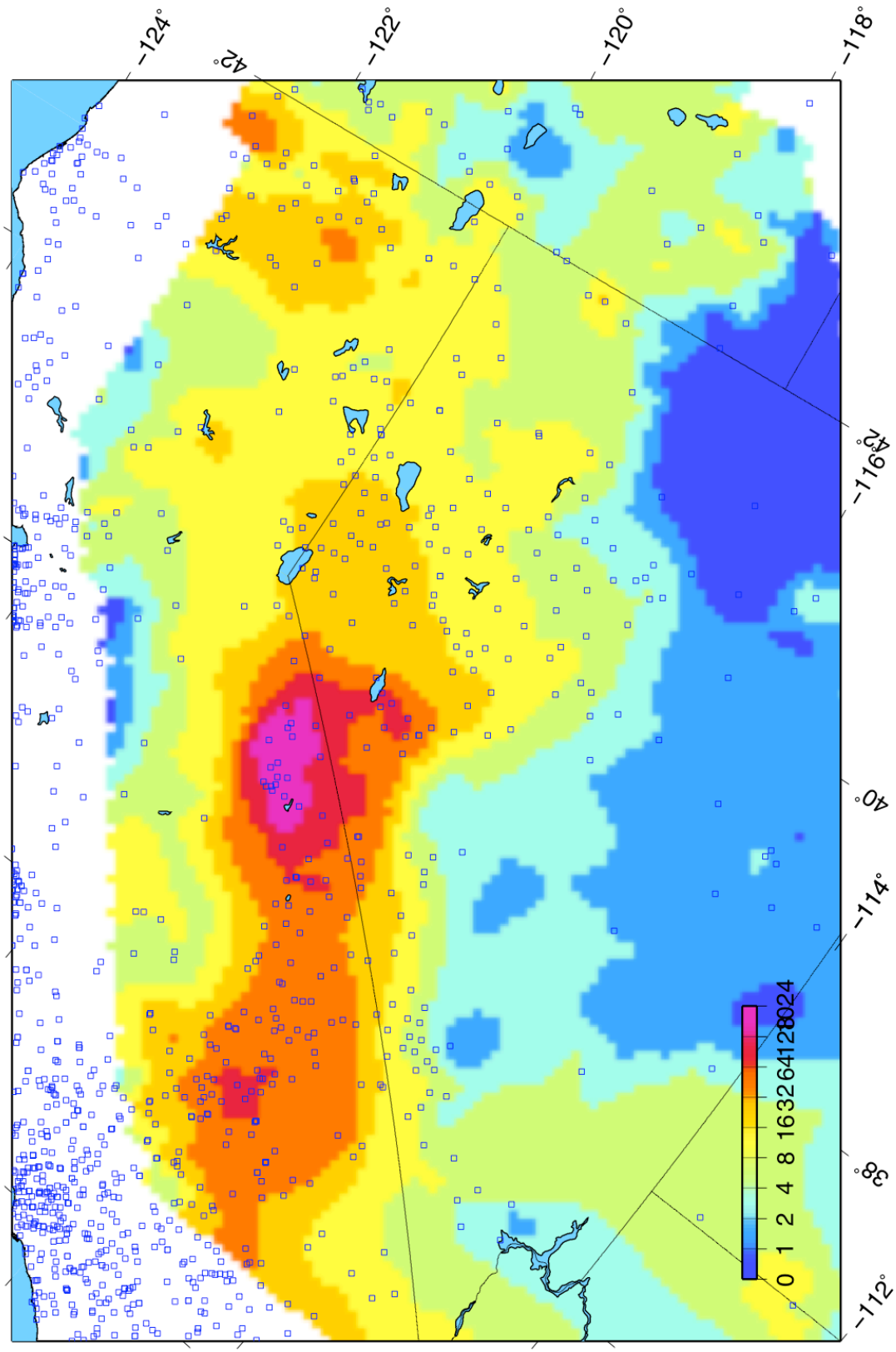

Figure 3. Map showing the intensity of the strain rate (includes shear and dilatation). Small black squares show locations of GPS sites used to constrain the model. Strain values are nanostrains. Projection is same as Figure 1.

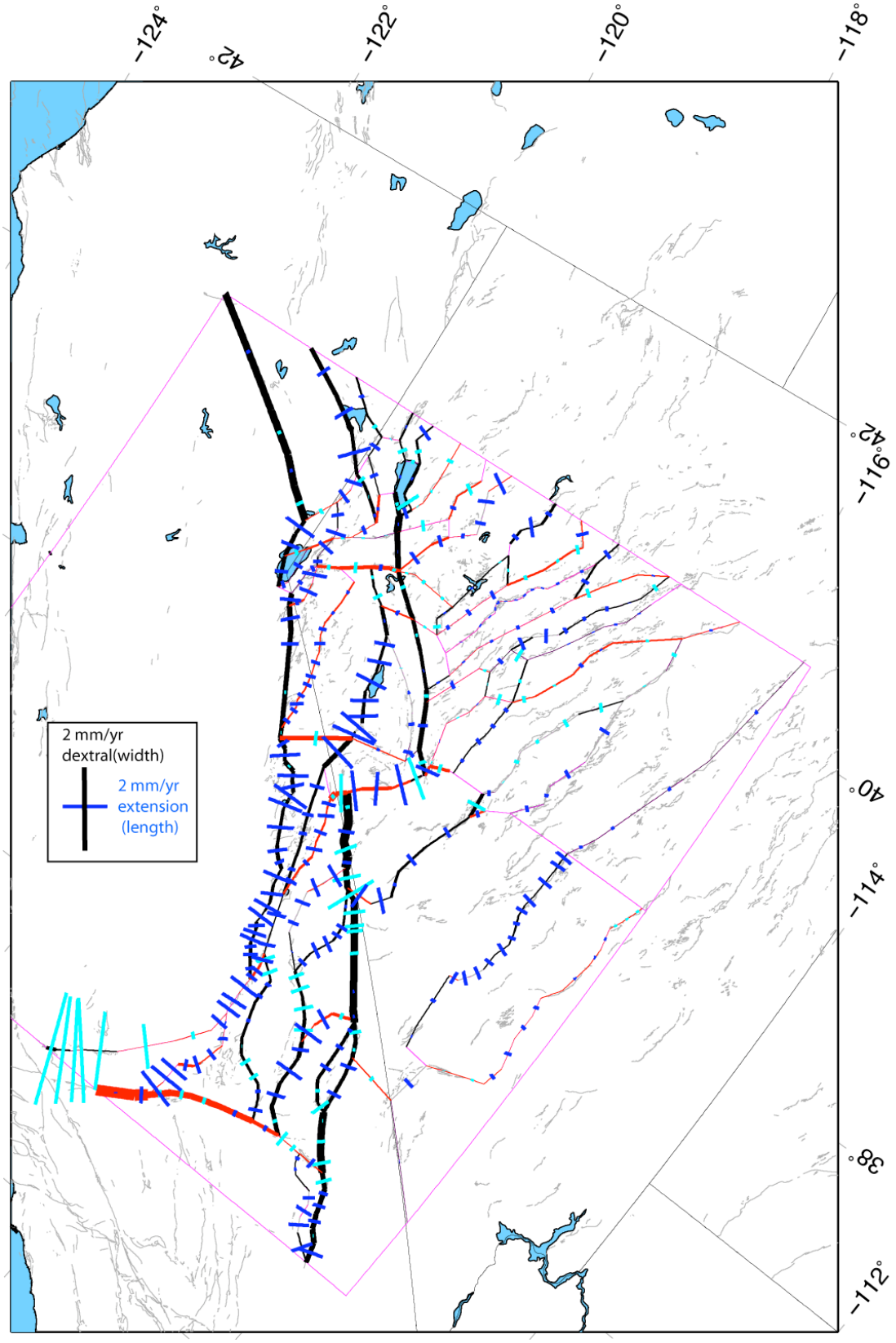

Figure 4. Slip rates on faults that bound the blocks in our model. Magenta lines show block boundaries. Thick black (red) lines indicate dextral (sinestral) slip rate by their width. Blue (cyan) lines indicate horizontal extensional (contraction) rate by their length. Light black lines are the traces of Quaternary and Holocene faults.

3.2. Block Models

Block modeling is advantageous in studies of crustal deformation because it allows integration of geodetic data with geologic and seismic data that constrain the geometry of fault surface traces and fault slip style. In this context blocks are essentially units of lithosphere that are completely bounded by faults so that they may move as rigid elements with respect to other blocks. Our formulation (*Hammond and Thatcher,* 2007) is similar to other block modeling strategies (e.g. *Bennett et al.,* 1996; *Prawirodirdjo et al.,* 1997; *Souter,* 1998*; McClusky et al.,* 2001; *McCaffrey,* 2002; *Meade and Hagar,* 2005) and accounts for the deformation that is observed at the surface near faults during the interseismic time frame. The technique essentially assumes that strain release on faults over geologic time will occur in patterns implied by velocity gradients during the interseismic time. During this time the faults that bound the blocks are locked at the surface and do not slip, except at great depth where motion is continuous. It is important to account for this so that all GPS velocities drive block motion, regardless of their proximity to faults. Because we estimate the long-term motion of the blocks (over many seismic cycles) the model also provides estimates of the relative motion between blocks, i.e. slip rates on the bounding faults.

However there are challenges in imaging slip rates when 1) faults are closely spaced, 2) faults have very low rates (order 0.1 mm/yr in some parts of our field area) and 3) slip rates vary by almost two orders of magnitude within the model. We have adopted a stochastically damped least-squares inversion technique that solves for block motions and slip rates simultaneously (*Hammond and Thatcher*, 2007), that allows us to place constraints on the slip rates when prior knowledge allows. This is useful, for example, when geologic studies constrain a slip rate at a point on a fault. In the model presented here, no prior knowledge of any individual fault slip rates was applied. However, a uniform prior uncertainty in slip rate of 1 mm/yr for all faults and a prior uncertainty in rotation rate of 1e-8 for all blocks were assumed. Residual velocities obtained after subtraction of the predictions of the model have an RMS of 0.86 mm/yr, while the normalized RMS is 1.28.

Features of the model include dextral slip that is distributed across the fault systems in the southern, central and northern Walker Lane, with significant slip occurring near the eastern margin of the WL. Normal extension is also well distributed across the southern WL, with rates of extension generally increasing to the west, and are highest at the Sierra Nevada range front. In general the North and South Death Valley faults have extension rates not significantly different that zero and dextral slip rates near 3.0 mm/yr. Where that system takes a more northerly strike near the Black Mountain fault zone extension rates become larger than the uncertainties, ~0.7 mm/yr. The Sierra Nevada Range front appears to accommodate 1.3-2.2 mm/yr of dextral slip and 0.7 – 1.2 mm/yr of extension, but locally higher extension rates where the strike of the fault is more northerly. Slip rates east of the Caron Sink in the central BRP north of latitude 39˚N have very low cumulative slip rates, most are not differentiable from zero in this model. Slip rates along the Mohawk Valley fault zone appear to be strictly dextral with no significant extension or contraction. Selected slip rates from this model are obtained by taking an average rate over a set of fault segments that define a specific fault (Table 1).

Table 1. Selected Fault Slip Rates from the Block Model.

Fault Name	Strike Slip Rate	Horizontal Contraction Rate
Mohawk Valley	-2.9+/-0.2	0.0+/-0.1
Honey Lake	-1.7+/-0.3	-1.3+/-0.3
West Tahoe	-1.6+/-0.4	-1.1+/-0.3
Wassuk	-0.9+/-0.2	-1.9+/-0.2
Sierra Nevada RF North (>38˚N)	-2.2+/-0.2	-0.7+/-0.2
Sierra Nevada RF Central (37˚-38˚N)	-1.4+/-0.1	-1.2+/-0.2
Sierra Nevada RF South (<37˚N)	-1.3+/-0.1	-0.9+/-0.1
Black Mountain	-1.5+/-0.3	-0.7+/-0.3
N. Death Valley	-2.8+/-0.2	0.4+/-0.2
S. Death Valley	-3.0+/-0.2	0.4+/-0.2
Fish Lake Valley	-3.6+/-0.2	0.0+/-0.2

Slip rates are in mm/yr, with 1-sigma uncertainty. Extension and dextral slip are reckoned negative.

3.3 Comparison between block models and strain maps

Block and continuum models are complementary approaches to understanding the patterns of crustal strain. To explore how well each technique can reproduce the results of the other, we take the predictions of the block model (rates of motion) and use these to compute a strain map using the same technique that was used to create Figure 3. This map (Figure 6 left) shows a very similar pattern of strain, with a concentration of strain near latitude 38˚N, longitude 120˚W, similar changes in width of the deforming zone, attenuation and widening of the deformation north of latitude 39˚N. However, when the predictions of the block model are given on a regular grid with spacing of 5km, and then these dense synthetic observations are used to build the strain map, a much different picture emerges (Figure 6 right). This synthetic strain map shows individual faults quite clearly, and resolves very low strain rates in the interior of blocks when there is sufficient distance between the bounding faults.

Thus if we have performed the block modeling correctly, one of the following is true: 1) if the earth is deforming in a manner similar to our present block model of crustal deformation, it may be possible to isolate some of the larger rigid blocks in the strain modeling approach by using denser deployments of GPS receivers, or 2) the block model is too simple, and its predictions are not smooth enough to account for the apparent smoothness of the GPS velocity field across the western BRP. Assertion 1) argues that a more extensive and more detailed deployment of GPS in this region will improve our estimates of the patterns of strain and rigidity in this region, since the detailed grid was able to reproduce the model pattern of strain. Assertion 2) argues that our representation of the structures is not sufficient, i.e. our block model requires more faults and/or assumed rigid blocks are actually internally deforming. This is likely true in particular areas, such as in the basins between Lake Tahoe and Walker Lane, where there are several basins with active faults, that we have not built into our model out of desire for a simpler representation, however in other locations (e.g. possibly between the Mohawk Valley and Honey Lake Faults) rigid blocks may be large enough to be detected. Another implication of this analysis is that block models, if they do include all the faults that actively accommodate deformation, will more accurately reproduce deformation patterns than strain maps built with incomplete GPS sampling of the deformation field. Therefore a general conclusion may be that

the best product will be obtained from 1) block models when geologic knowledge is complete even if geodetic knowledge is incomplete, or 2) from strain maps when geodetic knowledge is complete even if geologic knowledge is incomplete. In the western BRP we currently exist in a state somewhere in between these two end-members, demanding that we employ both complementary approaches.

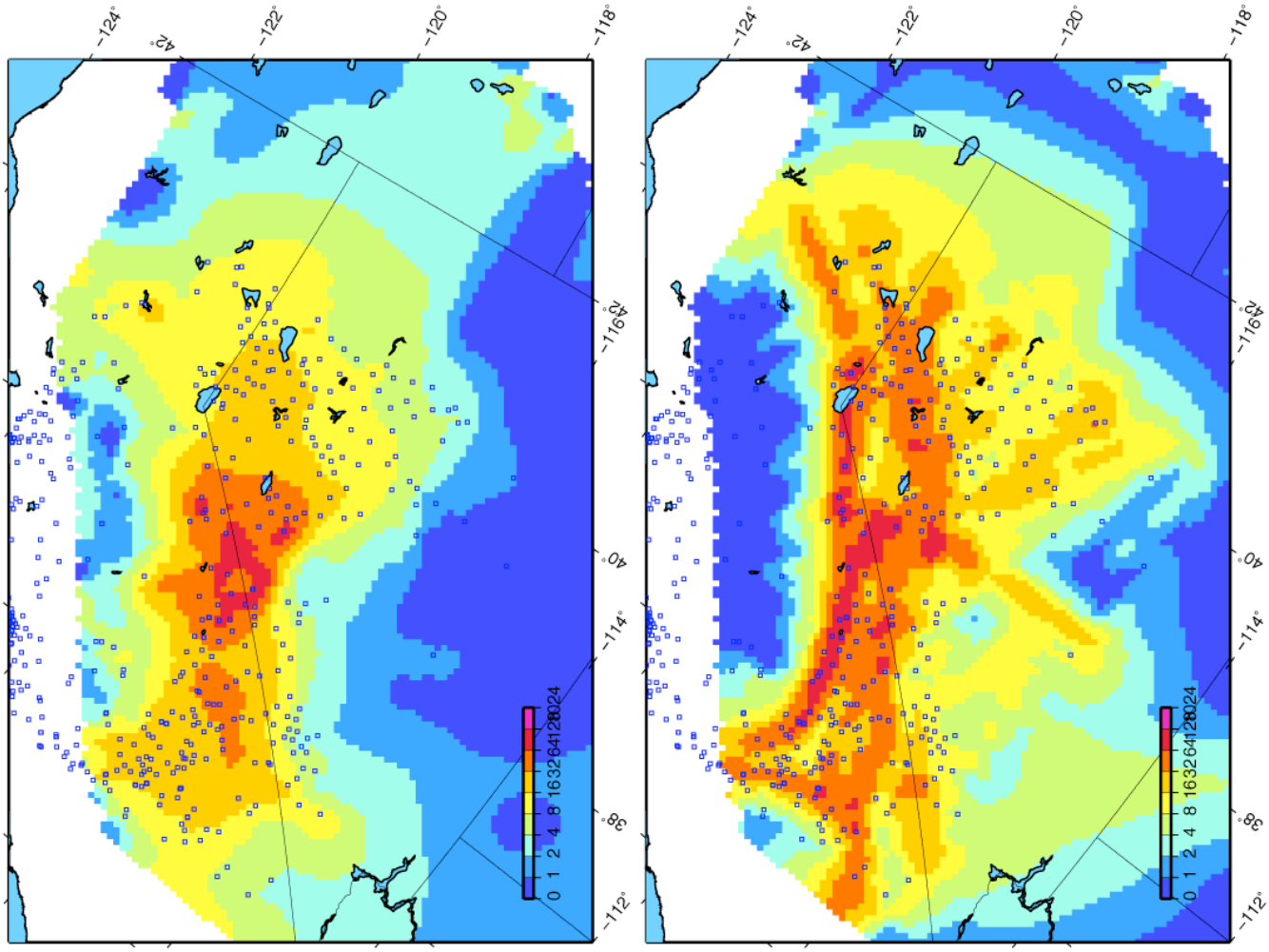

Figure 6. Strain maps obtained from the predictions of the block model at the GPS sites (left), and on a regular grid with spacing of 5 km (right). The squares show locations of sites used to constrain the block model. See text for discussion.

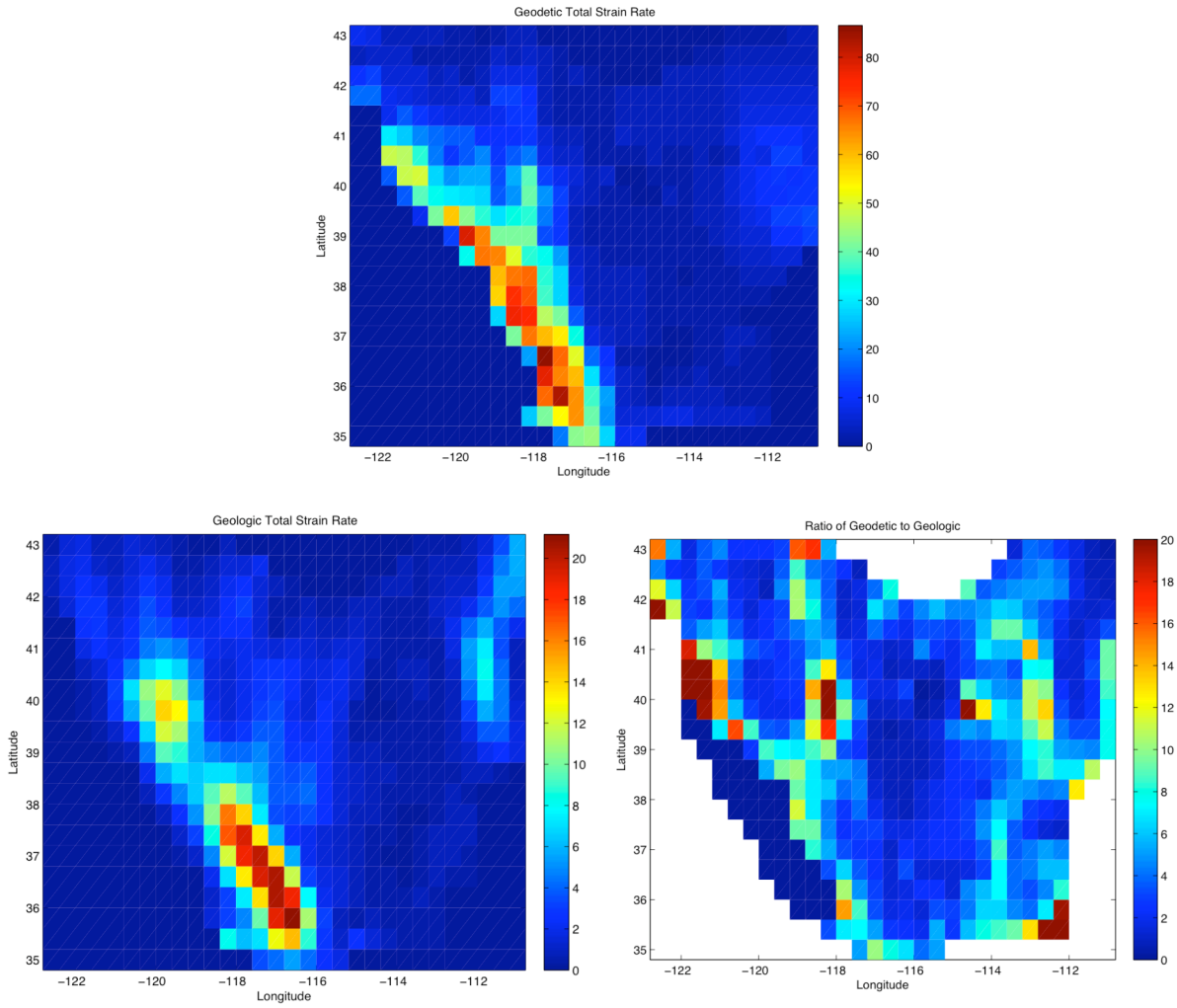

Figure 7. Map of total deformation moment as inferred from GPS geodesy (top), geologic data as present in the USGS QFFD (bottom left), and the ratio of those two, geodetic divided by geologic rate (bottom right). The top and middle panels were obtained using the same method as in Figure 3, except that the Sierra Nevada/Great Valley microplate was assumed to be rigid.

3.4 Comparison between geologic and geodetic estimates of strain rate

To compare the state of knowledge of deformation rate as inferred from GPS geodesy and geologic studies, we developed strain maps from both datasets (Figure 7). The strain rate was solved for in cells of dimensions 0.4˚x0.4˚ in latitude and longitude in the same method used to obtain Figures 3 and 6. We then took the ratio of the geodetic and geologic strain rates for each cell and plotted them in map view in the bottom panel of Figure 7 (*Hammond et al.,* 2008). The distribution of the ratio shows concentrations of the highest values where the geodetic deformation rate is significantly higher than the geologic estimate of deformation rate. First, near longitude 118˚W and latitude 40˚N the ratio is higher than elsewhere in the BRP. This is most likely attributable to ongoing postseismic relaxation from the CNSB earthquakes that has been discussed above. Second, the western margin of the BRP, immediately adjacent to the SNGV shows an elevated geodetic to geologic ratio, higher than the most of the BRP. The value is especially high near longitude 121˚W and latitude 40˚N where the Mohawk valley fault system has been inferred geologically (e.g. *Sawyer et al.,* 2005) to have a geologic slip rate of a few

tenths of a mm/yr, while the geodetic rates are approximately an order of magnitude higher (*Dixon et al., 2000*; *Hammond and Thatcher*, 2007). In general the geodetic values for strain rate are highest near the western edge of the BRP, but the geologic values are not, suggesting that the geologic data near the SNGV may be underestimating the strain rate. The central BRP shows a generally very low ratio. This is because the geodetically determined strain rates are near zero and many of the faults in the BRP were given reconnaissance quality values of 0.2 mm/yr for slip rates. Two other locations show high values for the moment rate ratio, in the central BRP near longitude 114˚W, latitude 40˚N and near longitude 112˚W and 35˚N, however these occur in places of very low geologic rate, and thus may be artifacts of numerical instability where the denominator of the ratio is near zero.

4. Conclusions

• Relatively high horizontal strain rates near Long Valley, CA have been inferred from both continuum and block models of western BRP deformation. These higher strain rates may indicate a relationship between active horizontal tectonics and the presence of the volcanic system, although the direction of cause/effect is not known.

• Comparisons between strain map and block modeling results for the western BRP suggest that the block model shown in Figure 4 may not be detailed enough in some areas. Alternatively a higher density of GPS sites is needed to resolve concentrations of strain from particular faults. Our ongoing NEHRP study of the Mohawk Valley fault zone will address this issue in detail.

• Comparisons between geologic (from the USGS QFFD) and from geodetic (from horizontal GPS) measures of strain suggest that the westernmost part of the BRP, within ~100 km of the SNGV, is where the disagreement between geodetic and geologic rates is greatest. This may be owing to fault slip rate estimates in the westernmost BRP being systematically too low, or to an insufficient number of paleoseismic/geologic studies that have quantified rates on active faults in this area.

• A general conclusion is that the best estimates of crustal strain will be obtained from 1) block models when geologic knowledge is complete even if geodetic knowledge is incomplete, or 2) from strain maps when geodetic knowledge is complete even if geologic knowledge is incomplete. In the western BRP we currently exist in a state somewhere in between these two end-members, demanding that we employ both complementary approaches.

5. References

Bell, J. W., Caskey, S. J., Ramelli, A. R., and Guerrieri, L., 2004, Pattern and rates of faulting in the central Nevada seismic belt, and paleoseismic evidence for prior belt-like behavior: Bulletin of the Seismological Society of America, v. 94, p. 1229-1254.

Bennett, R. A., Rodi, W., and Reilinger, R. E., 1996, Global Positioning System constraints on fault slip rates in southern California and northern Baja, Mexico: Journal of Geophysical Research, v. 101, p. 21,943 - 21,960.

Blewitt, G., 1989, Carrier phase ambiguity resolution for the Global Positioning System applied to geodetic baselines up to 2000 km: Journal of Geophysical Research, v. 94, p. 10,187-10,283.

—, 2006, The fixed point theorem of ambiguity resolution for precise point positioning of GPS networks: Theory and applications: Eos Transactions AGU Fall Meeting Supplement, v. 87(52) Fall Meet. Suppl. Abstract G43A-0977.

Blewitt, G., Argus, D. F., Bennett, R. A., Bock, Y., Calais, E., Craymer, M., Davis, J. L., Dixon, T. H., Freymueller, J. T., Herring, T. A., Johnson, D., Larson, K. M., Miller, E. L., Sella, G. F., Snay, R. A., and Tamissiea, M., 2005, A stable North America reference frame (SNARF): First release: UNAVCO-IRIS Joint Workshop.

Deng, J., Gurnis, M., Kanamoori, H., and Hauksson, E., 1998, Viscoelastic Flow in the lower crust after the 1992 Landers, California, Earthquake: Science, v. 282, p. 1689-1692.

Dixon, T. H., Miller, M., Farina, F., Wang, H., and Johnson, D., 2000, Present-day motion of the Sierra Nevada block and some tectonic implications for the Basin and Range province, North American Cordillera: Tectonics, v. 19, p. 1-24.

Frankel, A. D., Petersen, M. D., Mueller, C. S., Haller, K. M., Wheeler, R. L., Leyendecker, E. V., Wesson, R. L., Harmsen, S. C., Cramer, C. H., Perkins, D. M., and Rukstales, K. S., 2002, Documentation for the 2002 Update of the National Seismic Hazard Maps, Open File report 02-420, *in* Survey, U. S. G., ed.

Freed, A. M., Burgmann, R., and Herring, T., 2007, Far-reaching transient motions after Mojave earthquakes require broad mantle flow beneath a strong crust: Geophysical Research Letters, v. 34, p. -.

Gourmelen, N., and Amelung, F., 2005, Post-seismic deformation in the central Nevada seismic belt detected by InSAR: Implications for Basin and Range dynamics: Science, v. 310, p. 1473-1476.

Haines, J. A., and Holt, W. E., 1993, A proceedure for obtaining the complete horizontal motions within zones of distributed deformation from the inversion of strain rate data: Journal of Geophysical Research, v. 98, p. 12,057-12,082.

Hammond, W. C., Kreemer, C., and Blewitt, G., 2008, Geodetic constraints on contemporary deformation in the northern Walker Lane: 3, Postseismic relaxation in the Central Nevada Seismic Belt, Late Cenozoic Structure and Evolution of the Great Basin – Sierra Nevada Transition, Geological Society of America.

Hammond, W. C., Plag, H. P., and Kreemer, C., 2007, Postseismic relaxation from remote earthquakes observed in non-linearity of southern Basin and Range/Yucca mountain GPS time series, Seismological Society of America Annual Meeting, Kona, HI.

Hammond, W. C., and Thatcher, W., 2007, Crustal Deformation across the Sierra Nevada, Northern Walker Lane, Basin and Range Transition, western United States Measured with GPS, 2000-2004: Journal of Geophysical Research, v. 112, B05411, doi:10.1029/2006JB004625.

Hetland, E. A., and Hager, B. H., 2003, Postseismic relaxation across the Central Nevada Seismic Belt: Journal of Geophysical Research, v. 108, 2394, doi:10.1029/2002JB002257.

Kreemer, C., Blewitt, G., and Hammond, W. C., 2008a, Geodetic constraints on contemporary deformation in the northern Walker Lane: 2, velocity and tensor strain rate analysis: Late Cenozoic Structure and Evolution of the Great Basin – Sierra Nevada Transition.

Kreemer, C., Haines, J. A., Holt, W. E., Blewitt, G., and Lavallee, D., 2000, On the determination of the Global Strain Rate model: Earth Planets Space, v. 52, p. 765-770.

Kreemer, C., and Hammond, W. C., 2007, Geodetic constraints on areal-changes in the Pacific-North America plate boundary zone: What controls Basin and Range extension: Geology, v. v. 35, doi: 10.1130/G23868A.1, p. p 943-947.

Kreemer, C., Hammond, W. C., and Blewitt, G., 2008b, GPS velocity constraints on the kinematics of active tectonics in greater southern Nevada: GSA Cordilleran Section.

McCaffrey, R., 2002, Crustal block rotations and plate coupling, *in* Stein, S. A., Freymueller, Jeffrey, ed., AGU Geodynamics Series, AGU, p. 101-122.

McClusky, S. C., Bjornstad, S. C., Hagar, B. H., King, R. W., Meade, B. J., Miller, m. M., Monastero, F. C., and Souter, B. J., 2001, Present Day kinematics of the Eastern California Shear zone from a geodetically constrained block model: Geophysical Research Letters, v. 28, p. 3369-3372.

Meade, B. J., and Hagar, B. H., 2005, Block models of crustal motion in southern California constrained by GPS measurements: Journal of Geophysical Research, v. 110.

Pollitz, F. F., 2003, Transient rheology of the uppermost mantle beneath the Mojave Desert, California: Earth and Planetary Science Letters, v. 215, p. 89-104.

Pollitz, F. F., Wicks, C. W., and Thatcher, W., 2001, Mantle Flow Beneath a Continental Strike Slip Fault: Postseismic Deformation After the 1999 Hector Mine Earthquake: Science, v. 293, p. 1814-1818.

Prawirodirdjo, L., Bock, Y., McCaffrey, R., Genrich, J. F., Calais, E., Stevens, C., Puntodewo, S. S. O., Subarya, C., Rais, J., Zwick, P. C., and Fauzi, 1997, Geodetic observations of interseismic strain segmentation at the Sumatra subduction zone: Geophysical Research Letters, v. 24, p. 2601-2604.

Sawyer, T. L., Briggs, R. W., and Ramelli, A. R., 2005, Late Quaternary Activity of the Southern Mohawk Valley fault zone, northeastern California: Seismological Research Letters, v. 76, p. 248.

Souter, B. J., 1998, Comparisons of geological models to GPS observations in southern California: Unpub. Ph.D. thesis.

Williams, S. P. D., 2003, The effect of coloured noise on the uncertainties of rates estimated from geodetic time series: Journal of Geodesy, v. 76, p. 483-494.

Zumberge, J. F., Heflin, M. B., Jefferson, D. C., Watkins, M. M., and Webb, F. H., 1997, Precise point positioning for the efficient and robust analysis of GPS data from large networks: Journal of Geophysical Research, v. 102, p. 5005-5017.